KfK 3604
November 1983

Zur Porositätsabhängigkeit der Feldeigenschaften von Sinterwerkstoffen
Field Property Bounds for Porous Sintered Materials

P. Nikolopoulos, G. Ondracek
Institut für Material- und Festkörperforschung

Kernforschungszentrum Karlsruhe

KERNFORSCHUNGSZENTRUM KARLSRUHE
Institut für Material- und Festkörperforschung

KfK 3604

Zur Porositätsabhängigkeit der Feldeigenschaften von Sinterwerkstoffen

Field Property Bounds for Porous Sintered Materials

P. Nikolopoulos, G. Ondracek

Kernforschungszentrum Karlsruhe GmbH, Karlsruhe

Summary

The properties of two phase materials depend on their microstructure (concentration, geometry and geometrical arrangement of their phases). Theoretically derived equations provide upper and lower bounds, in-between which the properties of a two phase material may vary. The region of variation for the properties given by the bounds becomes closer with increasing degree of information about the microstructure. This is why Ist, IInd and IIIrd order bounds exist.

Up to now there was no possibility to transmit the calculation of bounds from two phase to porous materials due to the fact, that the existing lower bound equations fail for porosity as a second phase. These missing bounds of different order for the field properties of porous materials are derived in the present report and are compared with measured field property data

- in part I of the report for porous metals
- in part II of the report for porous ceramics
- in part III of the report for porous nuclear fuels

Part I is written in german, part II and III in English, so that the theoretical derivation is presented bilingually.

Zusammenfassung

Die Eigenschaften zweiphasiger Werkstoffe variieren mit ihrem Gefügeaufbau (Konzentration, Geometrie und geometrische Anordnung der Phasen). Durch theoretisch abgeleitete Gleichungen lassen sich obere und untere Grenzwerte berechnen, zwischen denen die Eigenschaften eines zweiphasigen Werkstoffes liegen müssen. Der durch diese Grenzwerte gegebene Variationsbereich für die Eigenschaften ist umso enger, je höher der Informationsgrad über den Gefügeaufbau ist. Man unterscheidet daher Grenzwerte I., II. und III. Ordnung.

Für poröse Werkstoffe ließen sich bisher untere Grenzwerte nicht berechnen, da die bekannten Grenzwertgleichungen für den Fall der Porosität als zweite Phase versagen. In der vorliegenden Arbeit werden diese

- bisher fehlenden - Grenzwertgleichungen verschiedener Ordnung für die Feldeigenschaften poröser Werkstoffe abgeleitet und

- im I. Teil des Berichtes mit gemessenen Feldeigenschaftswerten poröser Metalle
- im II. Teil des Berichtes mit gemessenen Feldeigenschaftswerten poröser keramischer Werkstoffe
- im III. Teil des Berichtes mit gemessenen Feldeigenschaftswerten poröser nuklearer Brennstoffe verglichen.

Der erste Teil ist in deutscher, Teil II und III des Berichts sind in englischer Sprache abgefaßt.

Sonderdruck aus:

ZEITSCHRIFT FÜR
METALLKUNDE
Herausgegeben von
DER DEUTSCHEN GESELLSCHAFT FÜR METALLKUNDE E.V.

DR. RIEDERER-VERLAG GMBH
POSTFACH 447
7000 STUTTGART 1

Zur Porositätsabhängigkeit der Feldeigenschaften von Sintermetallen

Panajotis Nikolopoulous* und Gerhard Ondracek**

(* Universität Patras, Griechenland und ** Kernforschungszentrum und Universität Karlsruhe, Postfach 3640, D-7500 Karlsruhe 1)

Von den vorhandenen oberen Grenzwertgleichungen I., II. und III. Ordnung zur Beschreibung der Feldeigenschaften (elektrische und thermische Leitfähigkeit, magnetische Permeabilität) poröser Werkstoffe ausgehend werden die zugehörigen unteren Grenzwertgleichungen abgeleitet. Wie der Vergleich mit experimentellen Feldeigenschaftswerten poröser Metalle zeigt, werden diese mit den aus Grenzwertgleichungen berechneten Grenzkurven gut erfaßt.

The Porosity Effect on the Field Properties of Sintered Metals

Based upon the available I., II. and III. order upper bound equations describing the field properties (electrical and thermal conductivity, magnetic permeability) of porous materials the respective lower bound equations have been derived. As the comparison between calculated bounds and experimental field property values points out there exists good fitting between measured quantities and theoretical curves.

Über Kontinuumstheorie und Grenzwertkonzept wurden Grenzwertgleichungen I. und II. Ordnung für zweiphasige Werkstoffe abgeleitet, die deren Feldeigenschaftswerte (thermische und elektrische Leitfähigkeit, magnetische Permeabilität) in Abhängigkeit von der Phasenkonzentration zwischen Grenzkurven einbinden[1]). Für poröse Werkstoffe mit Poren als eine Phase (Φ_P = Feldeigenschaft des porösen Werkstoffes; Φ_M = Feldeigenschaft des porenfreien Materials; P = Porosität) ergeben sich als

- obere Grenzwertgleichung I. Ordnung

$$\Phi_P^{I} = \Phi_M\,(1-P) \tag{1}$$

- obere Grenzwertgleichung II. Ordnung

$$\Phi_P^{II} = \Phi_M\,\frac{2\,(1-P)}{2+P} \tag{2}$$

und unter Zuhilfenahme des Modellkonzeptes[1]) als

- obere Grenzwertgleichung III. Ordnung

$$\Phi_P^{III} = \Phi_M\,(1-P)^{3/2} \tag{3}$$

während alle unteren Grenzwertgleichungen versagen[2]).

Hier ist – ingenieurmäßig – durch den Ordnungsgrad ausgedrückt, daß

- der Werkstoff zweiphasig ist (*eine* Voraussetzung = Grenzwertgleichungen I. Ordnung, Kirchhoff-Ohm-Gesetze)

- der Werkstoff zweiphasig und isotrop ist (*zwei* Voraussetzungen = Grenzwertgleichungen II. Ordnung, Hashin-Shtrikman-Grenzen[2a])

- der Werkstoff zweiphasig und isotrop ist und Matrixstruktur (Einlagerungsgefüge) aufweist (*drei* Voraussetzungen = Grenzwertgleichung III. Ordnung[1]).

Andererseits ist mehrfach gezeigt worden, daß die allgemeine Gefügestruktur-Feldeigenschaft-Gleichung für zweiphasige Werkstoffe nach dem Modellkonzept mit den Voraussetzungen des Grenzwertkonzeptes die Grenzwertgleichungen I. und II. Ordnung liefert[1])[3])[4])[5]) und daher als Ausgangspunkt für den Versuch zulässig ist, mit ihrer Hilfe die fehlenden unteren Grenzwertgleichungen für poröse Werkstoffe abzuleiten.

Zunächst ist aus dem Modellkonzept unmittelbar einsichtig, warum die aus dem Grenzwertkonzept folgenden unteren Grenzwertgleichungen im Porenfall versagen müssen:

In der Regel können Poren hinreichend gut durch Rotationsellipsoide beschrieben werden (z = Rotationsachse, x = Nebenachse), wie dies im Modellkonzept geschieht. Dann aber entsprechen die unteren Grenzkurven im Modellkonzept Werkstoffen mit scheibenförmigen Poren[1]) bis [6]). Für diese gilt $z/x = 0$, was gleichberechtigt entweder durch $z \to 0$ oder $x \to \infty$ erreicht wird. Poren mit unendlicher Nebenachse ($x \to \infty$) aber desintegrieren den Werkstoff, seine Feldeigenschaften werden bei jeder Porosität Null. Damit wird die Frage nach der realen statt fiktiven scheibenförmigen Porenform gleichbedeutend mit der Frage nach den unteren Grenzwertgleichungen.

Die allgemeine Gefügestruktur-Feldeigenschafts-Gleichung für den porösen Werkstoff[2])[3])[6]) liefert die effektive Feldeigenschaft (Φ_P) als Funktion der Feldeigenschaft der festen Phase ($\Phi_M \triangleq$ Feldeigenschaft des porenfreien Werkstoffs), der Porosität (P), Porenform (F) und -orientierung ($\cos^2\alpha$)[1])[2])[7])[8]):

$$\Phi_P = \Phi_M\,(1-P)^{\frac{\cos^2\alpha\,(3F-1)-2F}{2F\,(F-1)}}. \tag{4}$$

Um die zentrale Frage nach der realen Porenform praxisrelevant zu beantworten, wird hier auf die pulvertechnologische Entstehungsgeschichte der Porenform zurückgegriffen.

Die treibende Kraft im Sinterprozeß ist die Verringerung der „inneren" Oberflächenenergie. Bei geschlossener Porosität gilt

$$\Delta G = N \cdot \bar{S} \cdot \gamma \tag{5}$$

(ΔG = „innere" Oberflächenenergie; N = Anzahl der Poren;

$\bar{S}$ = mittlere Oberfläche einer Pore; γ = spezifische Oberflächenenergie = temperaturabhängige Materialgröße).

Im isothermen Sinterprozeß versucht der Werkstoff, seine „innere" Oberflächenenergie zu minimieren, wobei zwei zeitabhängige Prozesse parallel ablaufen:

- die Verringerung des Porenvolumens (Änderung der Porenzahl und -größe) durch Materialtransport.
- die Änderung der Porenform.

Der ideale Endzustand wäre der theoretisch dichte Sinterwerkstoff, der jedoch in der Praxis in aller Regel nicht erreicht wird. Läßt man im Gedankenexperiment die beiden o.a. Prozesse einmal hintereinander ablaufen, so bedeutet dies für eine einzelne Pore, daß sich zunächst ein konstantes Restvolumen einstellt und danach die Porenform in Richtung minimaler Oberfläche pro Volumen verändern wird. Die folgenden Betrachtungen gelten ausschließlich dieser Änderung der Porenform bei konstantem Volumen.

Das Volumen (V) rotationsellipsoid beschriebener Poren ergibt sich zu

$$V = \frac{\pi}{6} zx^2. \tag{6}$$

Die Oberfläche (S) errechnet sich:

- für Linsenporen (abgeplattete Rotationsellipsoide: $z/x < 1$) aus

$$S = \frac{\pi}{2}\left[x^2 + \frac{z^2}{\sqrt{1-(z/x)^2}} \ln \frac{1+\sqrt{1-(z/x)^2}}{z/x}\right] \tag{7}$$

- für Eiporen (gestreckte Rotationsellipsoide: $z/x > 1$) aus

$$S = \frac{\pi}{2}\left[x^2 + \frac{z^2 \arcsin \sqrt{1-(z/x)^2}}{\sqrt{1-\frac{1}{(z/x)^2}}}\right]. \tag{8}$$

Der Zustand minimaler Oberflächenenergie (ΔG_o) als Funktion der Porenform wird mit der Kugelpore ($z/x = 1$) erreicht. Normiert man für konstantes Porenvolumen auf diesen Zustand, so erhält man für die Funktion

$$\frac{\Delta G}{\Delta G_o} = \frac{S}{S_o} = f(z/x) \tag{9}$$

mit den Gln. (7) und (8) die in Bild 1 angegebenen Werte. Die Kurve zeigt, daß im Bereich kleiner Achsenverhältnisse geringfügige Formänderungen die Oberfläche – und damit Oberflächenenergie – sehr stark reduzieren. Der Kurvenverlauf kann in diesem Bereich durch die Funktion

$$\frac{S}{S_o} = 0.517 \left(\frac{z}{x}\right)^{-0.659} \tag{10}$$

mit guter Genauigkeit (≦1 % Abweichung gegenüber den Werten in Bild 1) beschrieben werden. Erst oberhalb $z/x = 0.1$ werden die Abweichungen rasch größer. In technischen Sinterprozessen darf daher erwartet werden, daß rotationsellipsoide Porenformen mit einem Achsenverhältnis $z/x = 0.1$ in aller Regel erreicht werden. Erst dann verlangsamt sich der Umformungsprozeß in Richtung sphärische Pore und kommt praktisch je nach den Sinterbedingungen zwischen Linsen-($z/x \geqq 0{,}1$) und Kugelporen ($z/x = 1$) zum Stillstand.

Wie Untersuchungen des Kurvenverlaufs über die erste Ableitung $d(S/S_o)/d(z/x)$ ergeben haben, sind die Energieänderungen $d(\Delta G/\Delta G_o) \cong d(S/S_o)$ bei Änderung der Form $d(z/x)$ für Werte von $z/x > 1$ denjenigen im Bereich $0{,}1 \leqq z/x \leqq 1$ vergleichbar. Quasizylindrische Porenformen (Porenkanäle) sind daher etwa als ebenso stabil anzusehen wie Linsenporen ($z/x \geqq 0{,}1$).

Gefügeanalytische Untersuchungen der Porenformen in Sintereisen bestätigen das obige Ergebnis: alle Poren hatten Linsenform mit Achsenverhältnissen $0{,}1 \leqq z/x \leqq 1$[16]). Mit diesem unteren Grenzwert des Achsenverhältnisses ($z/x = 0{,}1$) ergibt sich der – reale – Formfaktor für die unteren Grenzwertgleichungen poröser Werkstoffe zu $F = 0{,}0696$[1]).

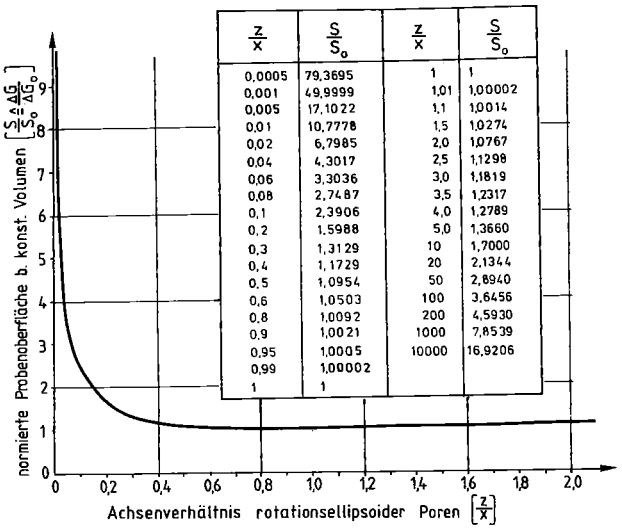

$\frac{z}{x}$	$\frac{S}{S_o}$	$\frac{z}{x}$	$\frac{S}{S_o}$
0,0005	79,3695	1	1
0,001	49,9999	1,01	1,00002
0,005	17,1022	1,1	1,0014
0,01	10,7778	1,5	1,0274
0,02	6,7985	2,0	1,0767
0,04	4,3017	2,5	1,1298
0,06	3,3036	3,0	1,1819
0,08	2,7487	3,5	1,2317
0,1	2,3906	4,0	1,2789
0,2	1,5988	5,0	1,3660
0,3	1,3129	10	1,7000
0,4	1,1729	20	2,1344
0,5	1,0954	50	2,8940
0,6	1,0503	100	3,6456
0,8	1,0092	200	4,5930
0,9	1,0021	1000	7,8539
0,95	1,0005	10000	16,9206
0,99	1,00002		
1	1		

Bild 1. Normierte Porenoberfläche und Achsenverhältnisse von rotationsellipsoiden Poren.

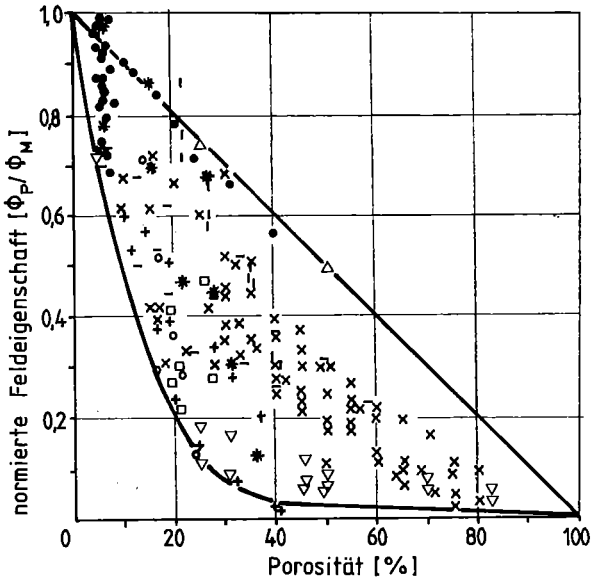

Bild 2. Feldeigenschaften von nichtisotropen porösen Sintermetallen.

——— Grenzkurven I. Ordnung

Thermische Leitfähigkeit □ Bronze[9]), ○ Cu[10]), △ Ni[11]), ▽ rostfreier Stahl[12]).

Elektrische Leitfähigkeit + Fe[13])[14]), × Nickellegierung[15]), – rostfreier Stahl[15]), I Ni[16]), * Cu[17]).

Magnetische Permeabilität ● Fe[6])[18]).

Im Modellkonzept entsprechen Gefügestrukturen mit folgenden Form- und Orientierungsfaktoren[1) bis 4)6)] der

- oberen Grenzwertgleichung I. Ordnung:

$$F = 0;\ \cos^2\alpha = 0$$

(Lösung von Gl. (4) über l'Hospital-Regel)

oder

$$F = 0{,}5;\ \cos^2\alpha = 1$$

- oberen Grenzwertgleichung II. Ordnung:

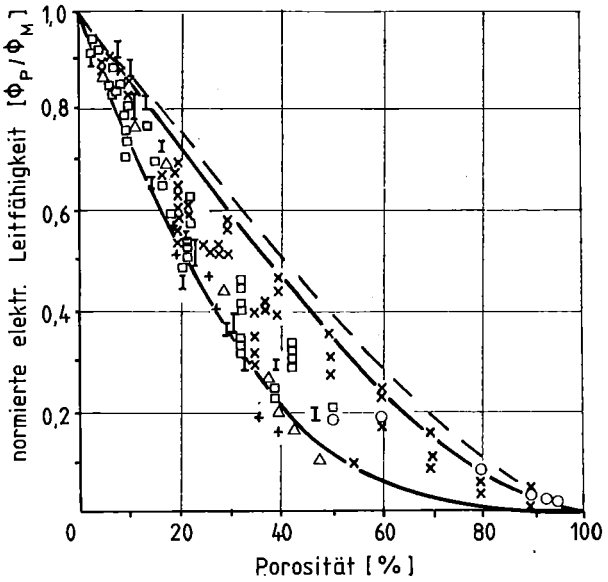

Bild 3. Elektrische Leitfähigkeit von isotropen porösem Metall.

-------- obere Grenzkurve II. Ordnung
——— Grenzkurven III. Ordnung

+ Bronze[9)], I Cu[14)19)20)], □ Stahl/Fe[6)16)19)21)], O Mo[22)], △ Ni[23)], × W[24)].

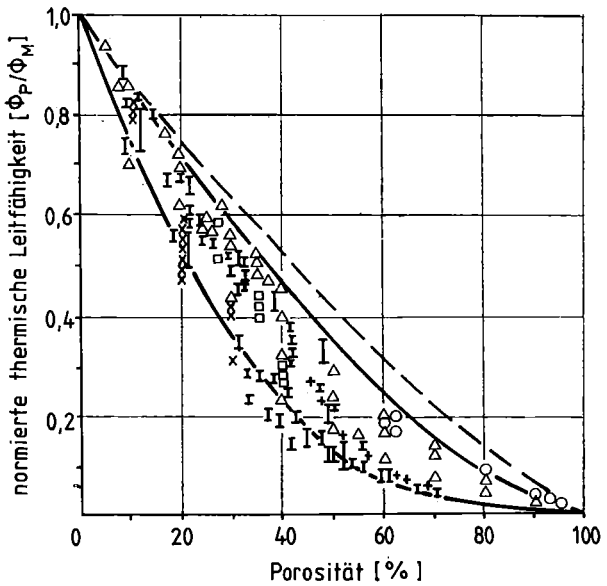

Bild 4. Thermische Leitfähigkeit von isotropen porösen Metallen.

----- obere Grenzkurve II. Ordnung
——— Grenzkurven III. Ordnung

I Stahl/Fe[16)19)25) bis 29)], × Cu[19)], O Mo[18)22)], △ W[24)30) bis 33)], □ Ni[16)], + Be[34)].

$$F = 0;\ \cos^2\alpha = \frac{1}{3}$$

- oberen Grenzwertgleichung III. Ordnung:

$$F = \frac{1}{3};\ \cos^2\alpha = \frac{1}{3}$$

Für die unteren Grenzwertgleichungen der Feldeigenschaften poröser Werkstoffe sind die Formfaktoren durch den oben ermittelten Formfaktor ($F = 0{,}0696$) zu ersetzen und zusammen mit den entsprechenden Orientierungsfaktoren in Gl. (4) einzusetzen. Damit ergibt sich in ingenieurmäßiger Näherung

- die untere Grenzwertgleichung I. Ordnung der Feldeigenschaften poröser Werkstoffe ($F = 0{,}0696$; $\cos^2\alpha = 1$)

$$\Phi_{PI} = \Phi_M\,(1-P)^7 \qquad (11)$$

- die untere Grenzwertgleichung II. Ordnung der Feldeigenschaften poröser isotroper Werkstoffe ($F = 0{,}0696$; $\cos^2\alpha = 1/3$)

$$\Phi_{PII} = \Phi_M\,(1-P)^3 \qquad (12)$$

- die untere Grenzwertgleichung III. Ordnung der Feldeigenschaften poröser isotroper Werkstoffe mit geschlossenen (diskontinuierlich eingelagerten) Poren ($F = 0{,}0696$; $\cos^2\alpha = 1/3$)

$$\Phi_{PIII} = \Phi_M\,(1-P)^3. \qquad (13)$$

Wie bei zweiphasigen Werkstoffen auch fallen die unteren Grenzkurven II. und III. Ordnung zusammen[1)].

Es sei hier noch der Vollständigkeit halber darauf hingewiesen, daß sich der Formfaktor für die obere Grenzkurve III. Ordnung auch herleiten läßt, wenn man in Gl. (4) den Orientierungsfaktor für isotrope Gefüge ($\cos^2\alpha = 1/3$) einsetzt und differenziert:

$$\frac{\mathrm{d}\,(\Phi_P/\Phi_M)}{\mathrm{d}F} = (1-P)^{\frac{3F+1}{6F(1-F)}}\left[\frac{3F^2+2F-1}{6F^2\,(1-F)^2}\right]\ln(1-P). \qquad (14)$$

Für $\mathrm{d}(\Phi_P/\Phi_M)/\mathrm{d}F = 0$ wird $F_{max} = 1/3$, womit sich aus Gl. (4) ($F = 1/3$; $\cos^2\alpha = 1/3$) (Gl. (3) ergibt.

Zum Vergleich zwischen theoretischen Grenzkurven und experimentellen Werten sind in Bild 2 die den Gln. (1) und (11) entsprechenden Grenzkurven I. Ordnung mit denjenigen Meßwerten der Feldeigenschaften poröser Sintermetalle verglichen, die keine isotrope Porenstruktur voraussetzen. Bild 3 und 4 zeigen den Vergleich experimenteller Werte der elektrischen und thermischen Leitfähigkeit von isotropen Sintermetallen mit den Grenzkurven II. und III. Ordnung gemäß Gln. (2), (3) und (12). Inzwischen durchgeführte Vergleiche bei porösen keramischen Werkstoffen und Graphit zeigen eine ähnlich gute Erfassung der Meßwerte durch die Grenzkurven[35)].

Herr Dipl.-Ing. Peter Klein hat wesentlich zur Auswertung, Herr Dipl.-Phys. Schust zur Erfassung der experimentellen Werte beigetragen, Frau Triplett hat das Manuskript geschrieben. Die Autoren bedanken sich für diese Hilfe.

Literatur

1) G. ONDRACEK, Metall **36** (1982) 523.
2) G. ONDRACEK, Z. Werkstofftechnik **8** (1977) 220, 280.

[2a]) Z. HASHIN und S. SHTRIKMAN, J. Appl. Phys. **33** – ID (1962) 3125.
[3]) G. ONDRACEK und B. SCHULZ, Ber. d. Kernforschungszentrum Karlsruhe, KFK 2171 (1974).
[4]) G. ONDRACEK und P. NIKOLOPOULOS, Proc. Int. Powder Metallurgy Conf., Florenz (1982) 89.
[5]) B. SCHULZ, Dissertation, Universität Karlsruhe (1974) 29.
[6]) R. PEJSA, Dissertation, Universität Karlsruhe (1981) 91.
[7]) G. ONDRACEK, Acta Stereol. **1** (1982) 5.
[8]) G. ONDRACEK, Werkstoffkunde, expert-Verlag Grafenau (1979) 129.
[9]) S. GROOTENHUIS, N. T. POWELL und M. A. TYE, Proc. Phys. Soc. **65** (1952) 502.
[10]) A. G. WALTER und A. R. TROWELL, J. Mater. Sci. **6** (1971) 1044.
[11]) J. FRANCL und W. D. KINGERY, J. Am. Ceram. Soc. **37** (1954) 99.
[12]) F. F. LEZHENIN, I. N. SHURGAY, A. G. KOSTORNOV und M. S. SHEVCHUK, Int. J. Heat and Mass Transfer **9** (1977) 144.
[13]) V. A. DANILENKO und A. V. ZRYIN, Sov. Powder Met. Metal. Ceram. **50** (2) (1967) 120.
[14]) F. SAUERWALD und J. KUBIK, Z. Elektrochemie **38** (1932) 5.
[15]) A. G. KOSTORNOV, M. S. SHEVCHUK, F. F. LEZHENIN, und I. M. FEDORCHENKO, Sov. Powder Met. Metal. Ceram. **16** (1977) 194.
[16]) P. I. MAL'KO, V. F. NEMCHENKO, S. N. L'VOV und V. S. PUGIN, Sov. Powder Met. Metal. Ceram. **73** (1) (1969) 49.
[17]) H. H. HAUSNER, Powder. Met. Bull. **3** (1948) 4.
[18]) L. M. ANISHENKO und V. F. BREKHOVSKIKH, Sov. Powder Met. Metal Ceram. **13** (1974) 298.
[19]) J. C. KOH, A. FORTINI, Int. J. Heat and Mass Transfer **16** (1973) 2013.
[20]) P. W. TAUBENBLATT, Int. J. Powder Met. **5** (1969) 89.
[21]) E. R. LEHEUP und J. R. MOON, Powder Metall. **21** (1978) 1.
[22]) I. N. CHAPOROVA, R. CHERNYAVSKII, S. T. AGABABOVA und U. S. VSOVA, Nauchn. Trudy Vses. Nauch. Issled. Proekt. Inst. **13** (1973) 50.
[23]) N. GRUBE und R. SCHLECHT, Z. für Elektrochemie **44** (1938) 367.
[24]) D. FRANCOIS, C. TERRAZ, R. MAYER und H. PASTOR, Planseeber. **20** (1972) 185.
[25]) G. I. AKSENOV und R. ZABBAROV, Sov. Powder Met. Metal. Ceram. **54** (6) (1967) 458.
[26]) L. BICEROGLU, N. MUJUMDAR, N. VAN HEINIGEN und C. DOUGLAS, Int. J. Heat and Mass Transfer **3** (1976) 183.
[27]) C. JANUSZEWSKII, L. KHOKAR und N. MUJUMDAR, Int. J. Heat and Mass Transfer **4** (1977) 417.
[28]) V. I. KONONENKO, V. M. BARANOVSKII und V. P. DUSHECHENKO, Sov. Powder Met. Metal. Ceram. **63** (3) (1968) 175.
[29]) R. ZABBAROV, Inzh. Fiz. Zh. **13** (1967) 373.
[30]) R. KULCINSKI und P. WAGNER, J. Less-Common Met. **7** (1964) 383.
[31]) A. V. LOGUNOV, O. B. CHEVELA und A. F. SILAEV, Sov. Powder Met. Metal. Ceram. **13** (1974) 304.
[32]) S. N. L'VOV, P. I. MAL'KO, L. V. NEVSKAYA und V. F. NEMCHENKO, Sov. Powder Met. Metal. Ceram. **41** (5) (1966) 416.
[33]) A. V. PUSTOGAROV, G. N. MELNIKO, A. N. KOLESNICHENKO, V. D. DARAGAN und D. D. CHEPIGA, Poroshk. Metall. **13** (1974) 52.
[34]) V. F. BYKOVSKII, R. M. DUBININ und C. V. NICHKOV, Sov. Atomic Energy **45** (1978) 793.
[35]) P. NIKOLOPOULOS und G. ONDRACEK, J. Am. Ceram. Soc. **66** (1983) Nr. 8.

(Eingegangen am 24. April 1982)

Reprinted from the Journal of the American Ceramic Society, Vol. 66, No. 4, April 1983

Field-Property Bounds for Porous Sintered Ceramics

PANAJOTIS NIKOLOPOULOS

Department of Chemical Engineering, University of Patras, Greece

GERHARD ONDRACEK

University and Kernforschungszentrum Karlsruhe, Federal Republic of Germany

Three sets of equations provide upper and lower values bounding the experimentally obtained electrical and thermal conductivities as well as the magnetic permeabilities (≙"field properties") of porous ceramics. These equations are as I-order upper bound: $\phi_P=\phi_M(1-P)$ (ϕ_P=effective field property of the porous material, ϕ_M=field property of the nonporous material, P=porosity), and as I-order lower bound: $\phi_P=\phi_M(1-P)^7$. Closer bounds corresponding to isotropic porous materials are the II-order upper bound: $\phi_P^{II}=\phi_M[2(1-P)/(2+P)]$, and the II-order lower bound: $\phi_{PIII}=\phi_M(1-P)^3$. Even closer bounds, referring to isotropic porous materials containing closed, unconnected pores are the III-order upper bound: $\phi_P^{III}=\phi_M(1-P)^{3/2}$, and the III-order lower bound: $\phi_{PIII}=\phi_M(1-P)^3$.

I. Theory

TREATING the microstructure-field property correlation for two-phase materials on the basis of continuum principle and bound concept, I- and II-order bound equations have been derived demonstrating quantitatively that the field properties (thermal and electrical conductivity, magnetic permeability) of two-phase materials may be predicted as a function of phase concentration by the upper and lower bounds.[1,2] For porous materials, where pores represent one phase (ϕ_P=effective field property of the porous material, ϕ_M=field property of nonporous material, P=porosity) these equations provide, respectively, I- and II-order upper bounds (Eqs. (11) and (9), Table I), whereas the lower-bound equations fail.[3–5] The same is true for the case of III-order bounds (Eq. (7), Table I), which were originally derived on the basis of the model concept.[2] In this context the degree of order expresses the extent of information concerning the materials microstructure, e.g. that (1) the material is two-phased (*one* single supposition=I-order bounds according to the Kirchhoff-Ohm law), (2) the material is two-phased and isotropic (*two* suppositions=II-order bounds according to Hashin-Shtrikman[1]), and (3) the material is two-phased, isotropic, and matrix-microstructured (*three* suppositions=III-order bounds[2]).

It has also been pointed out that the general microstructure-field property equation for two-phase materials derived on the basis of continuum principle and model concept provides the same I- and II-order bound equations as the bound concept if the assumptions made in the bound concept are introduced into the model concept theory.[2,5–8] This is why it is considered justifiable to use the model-concept microstructure-field property equation for deriving the missing lower-bound equations for porous materials.

It then becomes immediately obvious why the bound-concept lower-bound equations fail in the case of pores. Usually pores can be described sufficiently well as spheroids (z=rotation axis, x=minor axis) and this has been done in the model concept. The derivation of bounds by that concept, however, results in lower bounds for porous materials with disk-shaped pores[2,4–8] for which the relation $z/x\to 0$ applies, the solutions being obtained without preference either by $z\to 0$ or by $x\to\infty$.

Pores formed by $x\to\infty$, however, disintegrate the material—its field properties drop to zero at any porosity! To ask for the real instead of the fictitious disk-shaped pore form, therefore, refers to the question of the lower-bound equations of porous materials.

The general (model) microstructure-field property equation

Received May 14, 1982; revised copy received August 24, 1982; approved October 7, 1982.

(Eq. (1)) in Table I for porous materials provides the effective field property (ϕ_p) as a function of the field property of the solid phase ($\phi_M \triangleq$ field property of the nonporous material), the porosity (P), pore shape (F), and pore orientation ($\cos^2\alpha$).[2,4,6,7]

To answer the question as to the real pore shape in a practical situation, the powder technological factors which influence the formation of the pores must be considered.

In all sintering steps, the driving force is caused by the tendency to reduce the "internal" surface energy, which is given for closed porosity by

$$\Delta G = N \cdot \bar{S} \cdot \gamma \qquad (12)$$

where ΔG="internal" surface energy; N=number of pores; $\bar{S}$=average pore surface; and γ=specific surface energy, a temperature-dependent materials quantity.

During isothermal sintering, the material therefore tries to minimize the internal surface area, where two time-dependent parallel actions take place by materials transport: (1) the reduction of pore volume (alteration of number and size of pores), and (2) the alteration of pore shape to give the smallest surface-to-volume ratios.

Table I. Microstructure-Field Property Equations for Porous Materials*

general equation	$\phi_P = \phi_M(1-P)^{\frac{1-\cos^2\alpha}{1-F} + \frac{\cos^2\alpha}{2F}}$ (1)	
spherical pores	$\phi_P = \phi_M(1-P)^{3/2}$ (2)	
cylindrical pores statistically directed to the field direction (pore channels in isotropic materials)	$\phi_P = \phi_M(1-P)^{5/3}$ (3)	
cylindrical pores oriented perpendicular and parallel (I) to the field direction (oriented pare channels)	$\phi_P^I = \phi_M(1-P)^2$ (4)	$\phi_P^I = \phi_M(1-P)$ (5)
III. order bounds	$\phi_{III\,P} = \phi_M(1-P)^3$ (6)	$\phi^{III}{}_P = \phi_M(1-P)^{3/2}$ (7)
II. order bounds	$\phi_{II\,P} = \phi_M(1-P)^3$ (8)	$\phi^{II}{}_P = \phi_M^{\frac{2(1-P)}{2+P}}$ (9)
I. order bounds	$\phi_{I\,P} = \phi_M(1-P)^7$ (10)	$\phi^{I}{}_P = \phi_M(1-P)$ (11)

*F=shape factor for pores; $\cos^2\alpha$=orientation factor; P=porosity (fractional); ϕ_p=effective conductivity of porous material; ϕ_M=conductivity of nonporous material; $\phi_{I,II,III}$=lower bounds for effective conductivities; $\phi^{I,II,III}$=upper bounds for effective conductivities.

The ideal final state would be a theoretically dense material, which however usually does not result in practice under real technological conditions. Considering that the two preceding processes in a hypothetical experiment follow each other in series for a single pore, it would mean that a constant pore volume is achieved first, followed by the alteration of pore shape to minimize the surface-to-volume ratio of the pores. Further considerations will be exclusively focused on this second step of shape alteration at constant pore volume.

The volume (V) of spheroidal pores follows from

$$V = (\pi/6)zx^2 \qquad (13)$$

whereas the surfaces (S) are given for lenticular pores (oblate spheroids: $z/x<1$) by

$$S = \frac{\pi}{2}\left[x^2 + \frac{z^2}{(1-(z/x)^2)^{1/2}} \ln \frac{1+[1-(z/x)^2]^{1/2}}{z/x}\right] \qquad (14)$$

and for egg-shaped pores (prolate spheroids: $z/x>1$) by

$$S = \frac{\pi}{2}\left[x^2 + \frac{zx \arcsin\left(1-\frac{1}{(z/x)^2}\right)^{1/2}}{\left(1-\frac{1}{(z/x)^2}\right)^{1/2}}\right] \qquad (15)$$

The state of minimum surface-to-volume ratio and, therefore, minimum surface energy (ΔG_0), is obtained with spherical pores ($z/x=1$). Normalizing the surface energy (ΔG) and surface at constant pore volume to that state provides

$$\Delta G/\Delta G_0 = S/S_0 = f(z/x) \qquad (16)$$

which, using Eqs. (14) and (15), results in the values given numerically in Table II. As their plot in Fig. 1 demonstrates, changes in shape in the left region for small axial ratios cause large reductions in surface — and surface energy — ratios, respectively. The slope of the curve in that region is well approximated by the function

$$S/S_0 = 0.513(z/x)^{-0.662} \qquad (17)$$

with high accuracy between $0.0001<z/x<0.1$ compared with the actual data given numerically and graphically (broad black line) in Fig. 1 and Table II ($\leq 1\%$ deviation). Above $z/x=0.1$, however, the accuracy decreases rapidly. This is why in sintering processes spheroidal pore shape with axial ratios of $z/x \approx 0.1$ may be expected to be achieved under normal technological conditions. From this axial ratio, depending on the sintering conditions, the shape-transformation process by vacancy transport (compare sketch, Fig. 1) will be slowed and will finally stop between lenticular ($z/x \ll 1$) and spherical ($z/x=1$) pores.

Investigating the slope of the S/S_0-z/x curve by its first derivation $|d(S/S_0)/d(z/x)|$, it becomes obvious that energy changes ($d(\Delta G/\Delta G_0) \simeq d(S/S_0)$), related to form alterations at axial ratios $z/x>1$, correspond to those existing in the axial ratio region $0.1<z/x<1$. This is why quasi-cylindrical pores (pore channels) must be considered to be as stable as lenticular pores ($0.1<z/x<1$).

Precise quantitative microstructural analyses of the pore shapes in sintered iron have clearly confirmed the preceding conclusion; real pores are always lenticular with axial ratios of $0.1<z/x<1$.[7] Using the lower limiting axial ratio ($z/x=0.1$), the real shape factor for the lower-bound equations of porous materials results in $F=0.0696$.[2]

In the model concept, upper-bound microstructures refer to the following shape and orientation factors[2,4-7]: (1) I-order upper bound: $F=0$; $\cos^2\alpha=0$ (solution of Eq. (4) only, using the l'Hospital rule) or $F=0.5$; $\cos^2\alpha=1$, (2) II-order upper bound: $F=0$; $\cos^2\alpha=1/3$, and (3) III-order upper bound: $F=1/3$; $\cos^2\alpha=1/3$.

Table II. Numerical Values of Equation (16)

z/x	S/S_0	z/x	S/S_0
0.0005	79.3695	1	1
0.001	49.9999	1.01	1.00002
0.005	17.1022	1.1	1.0014
0.01	10.7778	1.5	1.0274
0.02	6.7985	2.0	1.0767
0.04	4.3017	2.5	1.1298
0.06	3.3036	3.0	1.1819
0.08	2.7487	3.5	1.2317
0.1	2.3906	4.0	1.2789
0.2	1.5988	5.0	1.3660
0.3	1.3129	10	1.7000
0.4	1.1729	20	2.1344
0.5	1.0954	50	2.8940
0.6	1.0503	100	3.6456
0.8	1.0092	200	4.5930
0.9	1.0021	1 000	7.8539
0.95	1.0005	10 000	16.9206
0.99	1.00002		
1	1		

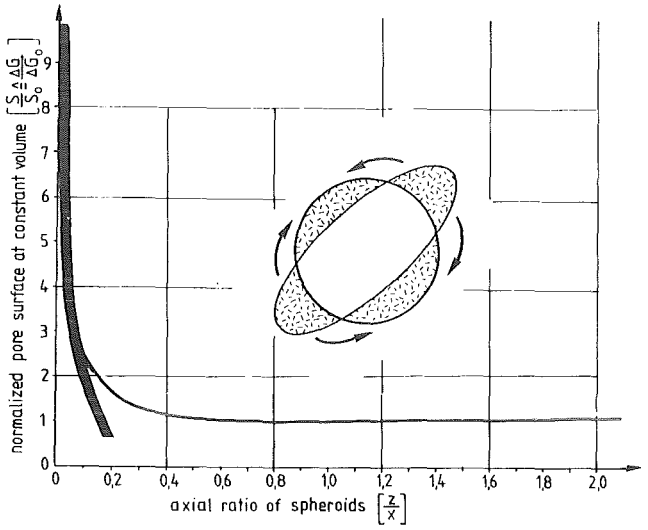

Fig. 1. Normalized pore surface and axial ratio.

Using these orientation factors and substituting the shape factors by the above-derived real shape factor in Eq. (4) results in engineering approaches for the I-order lower-bound equation for porous materials ($F=0.0696$, $\cos^2\alpha=1$; Eq. (10), Table 1), the II-order lower bound for isotropic porous materials ($F=0.0696$, $\cos^2\alpha=1/3$; Eq. (8), Table 1) and the III-order lower bound for isotropic porous materials with closed unconnected porosity ($F=0.0696$, $\cos^2\alpha=1/3$; Eq. (6), Table 1).

As in the case of materials consisting of two solid phases, the II- and III-order lower bounds are identical.[2] Additionally, it should be mentioned that the shape factor ($F_{max}=1/3$) for the III-order upper-bound equation (Eq. (3)) also follows by substituting the orientation factor for isotropic porous materials ($\cos^2\alpha=1/3$) in Eq. (4), differentiating and putting to zero:

$$\frac{d(\phi_p/\phi_M)}{dF}=(1-P)\frac{3F+1}{6F(1-F)}\left[\frac{3F^2+2F-1}{6F^2(1-F)^2}\right]\ln(1-P)=0 \quad (18)$$

If more-detailed information concerning pore shape and orientation are available, the lower and upper equations superimpose, resulting in one equation. This is given in Table I, for example, concerning spherical pores (Eq. (2), Table I) and cylindrical pores in various orientations (Eqs. (3), (4), and (5), Table I).

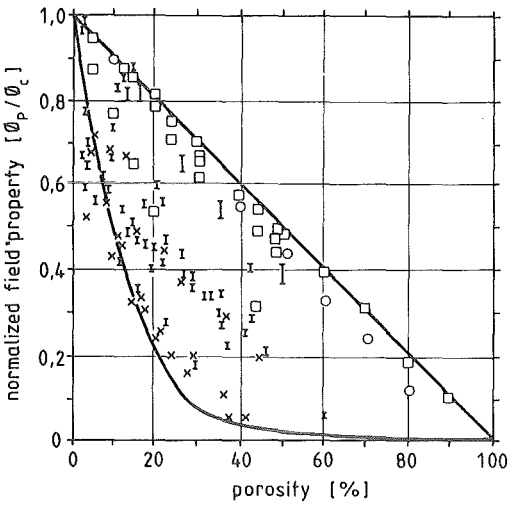

Fig. 2. Thermal conductivity and magnetic permeability of porous nonisotropic ceramics. Solid lines represent first-order bounds; data points represent experimental values of thermal conductivities for (□) Al_2O_3 (Refs. 9 and 10), (○) BeO (Ref. 9), and (I) minerals (Refs. 11, 12, 13, 14, and 15) and of magnetic permeability for (x) $Ni_{0.4}Zn_{0.6}Fe_2O_4$ (Ref. 16).

II. Measured Data and Calculated Bounds

In Figs. 2 and 3, the experimental values for the field properties of porous, not necessarily isotropic, sintered ceramics and graphite are compared with the respective I-order bounds corresponding to Eqs. (10) and (11). Figures 4 to 6 show the same comparison for the thermal and the electrical conductivity of porous but isotropic sintered ceramics and graphite. In the case of thermal conductivity of porous ceramics (Fig. 4), all experimental data refer to an isotropic microstructure, fitting therefore into the II-order bounds; but some of them systematically exceed the III-order upper bound, which suggests interconnected porosity. An isotropic solid-phase matrix structure, however, is confirmed by the measured electrical conductivities of porous ceramics in Fig. 5, and the measured conductivities of graphite in Fig. 6, which fit sufficiently well into the III-order bounds. Similar agreement between experimental and theoretical values has been obtained for porous sintered metals[5] and porous nuclear fuels.[31] Therefore, the derived bounds may be considered a reliable tool for calculating field properties of porous materials in an engineering context.

References

[1]Z. Hashin and S. Shtrikman, "A Variational Approach to the Theory of the Effective Magnetic Permeability of Multiphase Materials," *J. Appl. Phys.*, **33** [10] 3125–31 (1962).
[2]G. Ondracek,"On the Quantitative Microstructure-Field Property Correlation of Multiphase Materials," *Metall*, **36** [5] 523–31 (1982).
[3]P. Nikolopoulos and G. Ondracek, "Field Properties of Sintered Metals in Dependence on Porosity," *Z. Metallkunde*, **74** [1] 49 (1983).
[4]G. Ondracek, "On the Relationship Between the Properties and the Microstructure of Two-Phase Materials," *Z. Werkstofftechnik*, **8**, 220, 280 (1977).
[5]G. Ondracek and P. Nikolopoulos, "Correlation Between Properties and Porosity of Sintered Materials," *Proc. Int. Powder Metallurgy Conf.*, Florence, Italy, June 20–25, 1982.
[6]G. Ondracek and B. Schulz, "Contribution to the Conductivity of Multiphase Materials," *Ber. d. Kernforschungszentrums Karlsruhe*, KfK 2171 (1974).
[7]R. Pejsa, "On the Correlation Between Microstructure and Properties of Porous Materials," *Diss. Universität Karlsruhe*, 91 (1981).
[8]B. Schulz, "Field Properties of Two-Phase Materials and Their Dependence on the Microstructure," *Ber. d. Kernforschungszentrums Karlsruhe*, KfK 1988 (1974); p. 29.
[9]V. S. Bakunov, V. L. Balkevich, A. S. Vlasov, I. Ya. Guzman, E. S. Lukin, and D. N. Poluboyarinov, "Porous Ceramics out of Oxides," *Moscow. Metall.*, **2**, 232–60 (1977).
[10]J. Francl and W. D. Kingery, "Thermal Conductivity: IX, Experimental Investigation of Effect of Porosity on Thermal Conductivity," *J. Am. Ceram. Soc.*, **37** [2] 99–107 (1954).
[11]H. Clark, "The Effects of Simple Compression and Wetting on the Thermal Conductivity of Rocks," *Trans. Am. Geophys. Union*, **3**, 543–44 (1941).
[12]J. H. Huang, "Effective Thermal Conductivity of Porous Rocks," *J. Geophys. Res.*, **76** [26] 6420–27 (1971).

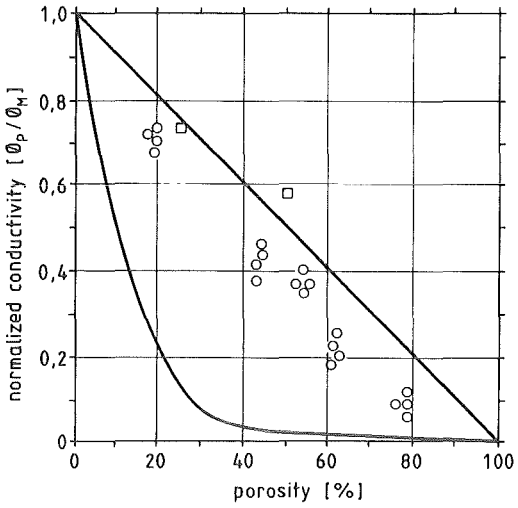

Fig. 3. Conductivity of porous carbon and graphite. Solid lines represent first-order bounds and data points experimental values of (□) thermal conductivity (Ref. 10) and (○) electrical conductivity (Ref. 17).

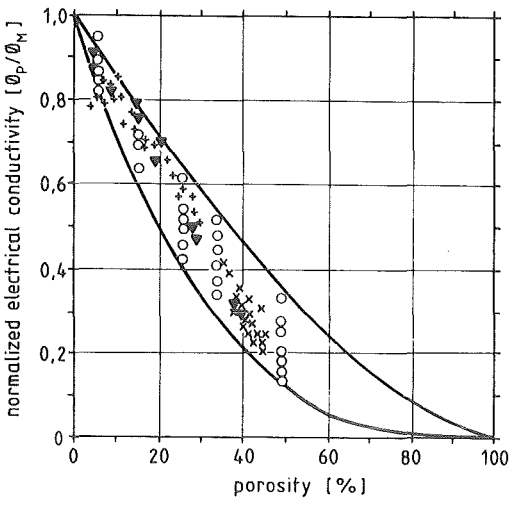

Fig. 5. Electrical conductivity of porous isotropic ceramics. Solid lines represent 3rd-order bounds and data points experimental values for (○) ZrO_2 (Ref. 23), (+) TiC (Ref. 24), (x) Ca_xMo_yC (Ref. 25), and (▼) TiN (Ref. 21).

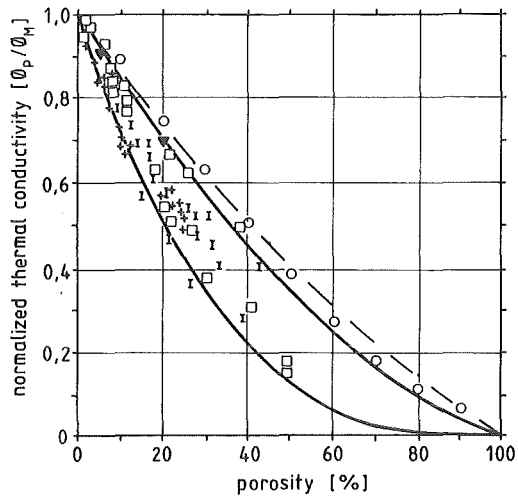

Fig. 4. Thermal conductivity of porous isotropic ceramics. Dashed line represents second-order bounds and solid line third-order bounds; data points represent experimental values for (□) Al_2O_3 (Refs. 14 and 18), (○) ZrO_2 (Ref.9), (+) B_4C (Refs. 19 and 20), (▼) TiN (Ref. 21), and (I) minerals (Ref. 22).

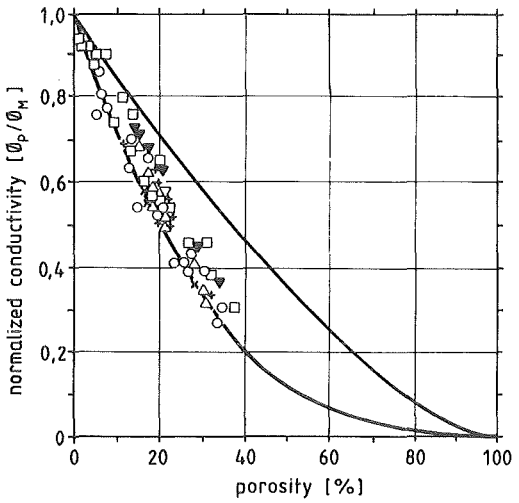

Fig. 6. Conductivity of isotropic porous carbon and graphite. Solid lines represent 3rd-order bounds; data points represent experimental values of thermal conductivity from (□) Ref. 26, (○) Ref. 27, (△) Ref. 28, (+) Ref. 29, and (x) Ref. 30 and of electrical conductivity from (▼) Ref. 28.

[13]E. C. Robertson and D. L. Peck, "Thermal Conductivity of Vesicular Basalt from Hawaii," *J. Geophys. Res.*, **79** [32] 4875–88 (1974).
[14]T. Saegusa, Y. Iida, N. Wakao, and K. Kamata, "Thermal Conductivities of Porous Solids," *J. Heat Transfer*, **3** [2] 47–52 (1974).
[15]W. Woodside and J. H. Messmer, "Thermal Conductivity of Porous Media: II, Consolidated Rocks," *J. Appl. Phys.*, **32** [9] 1699–706 (1961).
[16]H. Igarashi and K. Okazaki, "Effects of Porosity and Grain Size on the Magnetic Properties of NiZn Ferrite," *J. Am. Ceram. Soc.*, **60** [1–2] 51–54 (1977).
[17]E. A. Bel'skaya and A. S. Tarabanov, "Experimental Studies Concerning the Electrical Conductivity of High-Porosity Carbon-Graphite Materials," *J. Eng. Phys.*, **20** [4] 472–75 (1970).
[18]J. D. McClelland and L. O. Petersen, "Effect of Porosity on the Thermal Conductivity of Alumina," U.S. Atomic Energy Comm. NAA–SR–6473, 9 (1961).
[19]T. Iseki, M. Ito, H. Suzuki, and T. Honda, "Effect of Neutron Irradiation on Thermal Conductivity, Electric Resistivity and Thermal Expansion of Boron Carbide," *J. Nucl. Sci. Technol.*, **10** [6] 360–66 (1973).
[20]D. E. Mahagin, D. E. Baker, and J. L. Bates, "Boron Carbide Thermal Conductivity"; for abstract see *Am. Ceram. Soc. Bull.*, **52** [9] 718 (1973).
[21]M. I. Aivazov and I. A. Domashnev, "Influence of Porosity on the Conductivity of Hot-Pressed Titanium-Nitride Specimens," *Sov. Powder Met. Met. Ceram.*, **7**, 708–10 (1968).
[22]A. Sugawara and Y. Yoshizawa, "An Experimental Investigation on the Thermal Conductivity of Consolidated Porous Materials," *J. Appl. Phys.*, **33** [10] 3135–38 (1962).
[23]D. S. Rutman, A. F. Maurin, G. A. Taksis, and Yu. S. Toropov, "Relationship Between Electric Resistance of Zirconia Ceramics and Porosity," *J. Refract.*, **6**, 371–74 (1970).
[24]G. V. Samsonov and V. E. Matsera, "Powder Metallurgical Materials, Parts, and Coatings, Manufacture and Properties of Powder Metallurgical Refractory Compound Fibers and Porous Fiber Materials," *Sov. Powder Met. Met. Ceram.*, **11** [9] 719–23 (1972).
[25]E. M. Petrova, "Electrical Resistivity of Composite Materials," *Tekhnol. Poluch. Novykh. Mater.*, 24–30 (1973).
[26]J. E. Brocklehurst, R. G. Brown, K. E. Gilchrist, and V. Y. Labaton, "The Effect of Radiolytic Oxidation on the Physical Properties of Graphite," *J. Nucl. Mater.*, **35**, [2] 183–94 (1970).
[27]H. Matsuo, "Effect of Porosity on the Thermal Conductivity of Nuclear Graphite," *J. Nucl. Mater.*, **89** [1] 9–12 (1980).
[28]S. K. Rhee, "Discussion of Porosity Effects in Polycrystalline Graphite"; *J. Am. Ceram. Soc.*, **55** [11] 580–81 (1972).
[29]P. Wagner, J. A. O'Rourke, and P. E. Armstrong, "Porosity Effects in Polycrystalline Graphite," *J. Am. Ceram. Soc.*, **55** [4] 214–19 (1972).
[30]J. M. Hutcheon and M. S. T. Price, "Dependence of the Properties of Graphite on Porosity"; Proceedings of the Fourth Conference on Carbon (1959). Pergamon, New York, 1960.
[31]P. Nikolopoulos and G. Ondracek, "Conductivity Bounds for Porous Nuclear Fuels," *J. Nucl. Mater.*, 114 (1983).

Journal of Nuclear Materials 114 (1983) 231–233
North-Holland Publishing Company

CONDUCTIVITY BOUNDS FOR POROUS NUCLEAR FUELS

P. NIKOLOPOULOS

Department of Chemical Engineering, University of Patras, Greece

G. ONDRACEK

Institut für Material- und Festkörperforschung, Kernforschungszentrum Karlsruhe, Fed. Rep. Germany

Received 27 April 1982; accepted 2 August 1982

By treating the microstructure-field-property-correlation for a two-phase material on the basis of a continuum model concept [10–12] a general microstructure-field property equation was derived demonstrating, that the field properties (electrical and thermal conductivity, magnetic permeability) of two-phase matrix materials depend on the concentration, shape and orientation of the inclusions. Substituting the included phase particles by pores, results in a general equation for porous materials (table 1), which leads to special expressions for spherical porosity and cylindrical pores in various orientations (table 1).

In practice the exact determination of the pore structure is frequently considered to be difficult, time consuming and inaccurate. This is why the *bound concept* was used to predict the conductivity as a function of

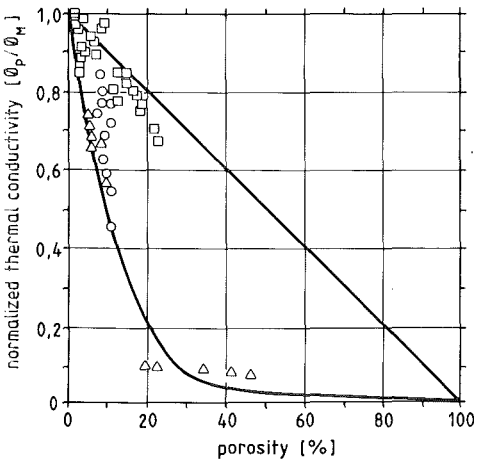

Fig. 1. Thermal conductivity of porous oxide nuclear fuels. — : I-order bounds; exp. values: □ UO_2 [2,16], ○ $(UP_4)O_2$ [8], △ ThO_2 [15,18].

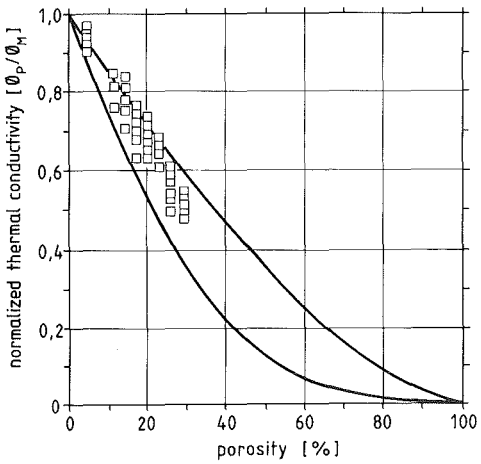

Fig. 2. Thermal conductivity of porous UN. – : III-order bounds, □ experimental values [6].

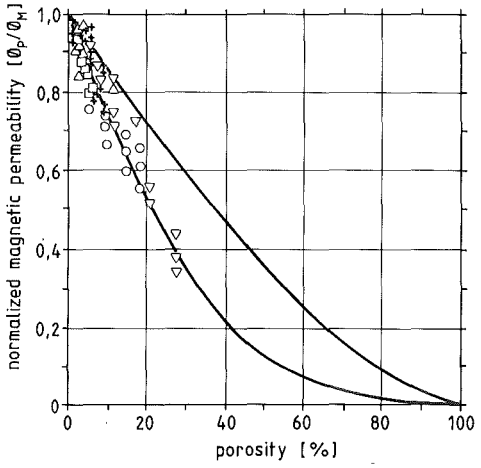

Fig. 3. Conductivity of porous UO_2. —: III-order bounds; exp. values: ○ [1], ▽ [3,4], □ [7], △ [17].

0022-3115/83/0000–0000/$03.00

Journal of Nuclear Materials 114 (1983) 231–233
North-Holland Publishing Company

CONDUCTIVITY BOUNDS FOR POROUS NUCLEAR FUELS

P. NIKOLOPOULOS

Department of Chemical Engineering, University of Patras, Greece

G. ONDRACEK

Institut für Material- und Festkörperforschung, Kernforschungszentrum Karlsruhe, Fed. Rep. Germany

Received 27 April 1982; accepted 2 August 1982

By treating the microstructure-field-property-correlation for a two-phase material on the basis of a continuum model concept [10–12] a general microstructure-field property equation was derived demonstrating, that the field properties (electrical and thermal conductivity, magnetic permeability) of two-phase matrix materials depend on the concentration, shape and orientation of the inclusions. Substituting the included phase particles by pores, results in a general equation for porous materials (table 1), which leads to special expressions for spherical porosity and cylindrical pores in various orientations (table 1).

In practice the exact determination of the pore structure is frequently considered to be difficult, time consuming and inaccurate. This is why the *bound concept* was used to predict the conductivity as a function of

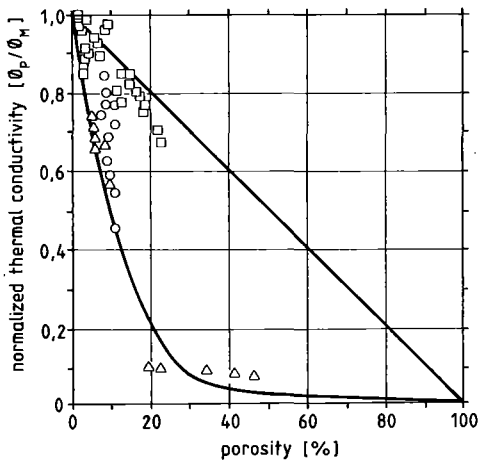

Fig. 1. Thermal conductivity of porous oxide nuclear fuels. — : I-order bounds; exp. values: □ UO_2 [2,16], ○ $(UP_4)O_2$ [8], △ ThO_2 [15,18].

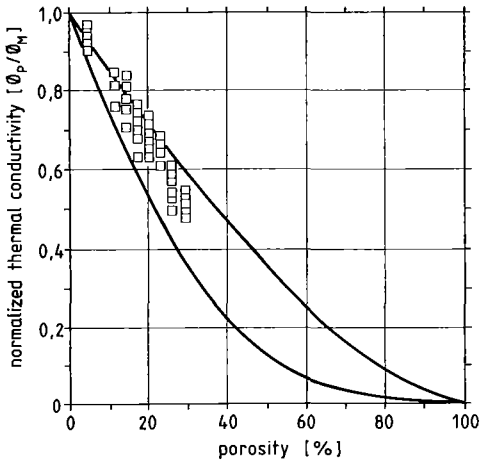

Fig. 2. Thermal conductivity of porous UN. – : III-order bounds, □ experimental values [6].

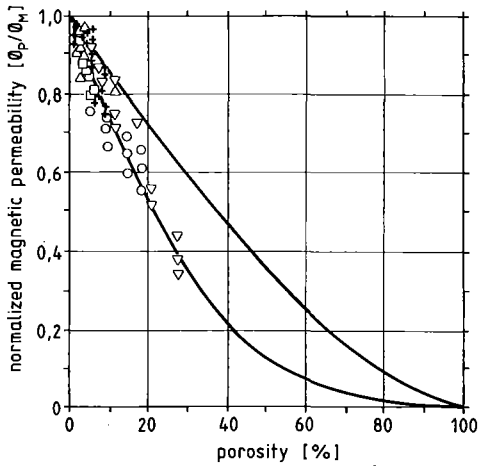

Fig. 3. Conductivity of porous UO_2. —: III-order bounds; exp. values: ○ [1], ▽ [3,4], □ [7], △ [17].

0022-3115/83/0000–0000/$03.00

Table 1
Microstructure-field property equations for porous materials

general equation	$\phi_P = \phi_M(1-P)^{\frac{1-\cos^2\alpha}{1-F} + \frac{\cos^2\alpha}{2F}}$ (1)	
spherical pores	$\phi_P = \phi_M(1-P)^{3/2}$ (2)	
cylindrical pores statistically directed to the field direction (pore channels in isotropic materials)	$\phi_P = \phi_M(1-P)^{5/3}$ (3)	
cylindrical pores oriented perpendicular ($\perp$) and parallel (I) to the field direction (oriented pore channels)	$\phi_P^{\perp} = \phi_M(1-P)^2$ (4)	$\phi_P^{I} = \phi_M(1-P)$ (5)
III. order bounds	$\phi_{III\,P} = \phi_M(1-P)^3$ (6)	$\phi^{III}{}_P = \phi_M(1-P)^{3/2}$ (7)
II. order bounds	$\phi_{II\,P} = \phi_M(1-P)^3$ (8)	$\phi^{II}{}_P = \phi_M\frac{2(1-P)}{2+P}$ (9)
I. order bounds	$\phi_{I\,P} = \phi_M(1-P)^7$ (10)	$\phi^{I}{}_P = \phi_M(1-P)$ (11)

(F = shape factor of the pores; $\cos^2\alpha$ = orientation factor; P = porosity (fractional); ϕ_P = effective conductivity of the porous material; ϕ_M = conductivity of the nonporous material; $\phi_{I,II,III}$ = lower bounds for effective conductivities; $\phi^{I,II,III}$ = upper bounds for effective conductivities.)

porosity without quantitative microstructural measurements within a certain margin of inaccuracy [5,9,10,11]. In this context (table 1)

I-order bounds refer to materials without any other microstructural information than that of being *porous*;

II-order bounds refer to *porous* and *isotropic* materials;

III-order bounds refer to *porous* and *isotropic* materials with exclusively *non-interconnected* (closed) porosity.

Whilst the derivation of the upper bounds permits us to state, that these bounds give definite maximum values and should not be exceeded by any measured data, the lower bounds are based on an engineering approach [14]. In fig. 1 the experimental values for the thermal conductivity of porous non-isotropic nuclear fuels are compared with the respective I-order bounds corresponding to eqs. (10) and (11). The same has been done in fig. 2 for porous but isotropic uranium mononitride

and in fig. 3 for the thermal as well as the electrical conductivity of porous but isotropic UO_2. Due to the isotropic nature of the porosity in figs. 2 and 3 the theoretical curves are III-order bounds refering to eqs. (6) and (7). Similar good agreement between bounds and measured values was obtained for porous sintered metals [9,13], porous graphite and ceramics [14].

References

[1] R.R. Asamoto, F.L. Anselin and A.E. Conti, J. Nucl. Mater. 29 (1969) 67.

[2] J. Belle, Uranium dioxide, US AEC Naval Reactors (1961).

[3] J.C. van Craeynest and J.P. Stora, J. Nucl. Mater. 37 (1970) 153.

[4] L.A. Goldsmith and J.A.M. Douglas, J. Nucl. Mater. 47 (1973) 31.

[5] Z. Hashin and S. Shtrikman, Phys. Rev. 130 (1963) 129.

[6] T. Kikuchi, T. Takahashi and S. Nasu, J. Nucl. Mater. 45 (1972/73) 284.

[7] J.R. MacEwan, R.L. Stoute and M.I.F. Notley, J. Nucl. Mater. 24 (1967) 109.

[8] H. Gibby, G. Lawrence, Proc. Am. Ceram. Soc., Winter Meeting (1971).

[9] P. Nikolopoulos and G. Ondracek, Z. Metallkunde (1982), submitted for publication.

[10] G. Ondracek, Z. Werkstofftechnik 8 (1977) 220, 280.

[11] G. Ondracek, Metall 36 (1982) 523.

[12] G. Ondracek and B. Schulz, Ber. d. Kernforschungszentrum Karlsruhe, KfK 2171 (1974).

[13] G. Ondracek and P. Nikolopoulos, Proc. Int. Powder Metallurgy Conf., Florence, Italy (June 20–25, 1982) p. 89.

[14] P. Nikolopoulos and G. Ondracek, J. Amer. Ceram. Soc. (1982) submitted for publication.

[15] M. Murabayashi, Y. Takahashi, J. Nasu, J. Nucl. Science and Techn. 6 (1969) 47.

[16] S.K. Ross, AECL 1096 (1960).

[17] J. Vogt, L. Grandell and U. Runfors, AB Atomenergi (Sweden) Int. Report, RMB-527 (1964).

[18] S.A. El-Fekey, M. El-Mamoon Jehia, M.N.A. El-Hakim, Powder Met. Int. 10/2 (1978) 90.